Supplement of Atmos. Chem. Phys., 20, 9249–9263, 2020
https://doi.org/10.5194/acp-20-9249-2020-supplement

Atmospheric Chemistry and Physics
Open Access
EGU

Supplement of

Simultaneous measurements of urban and rural particles in Beijing – Part 2: Case studies of haze events and regional transport

Yang Chen et al.

Correspondence to: Fumo Yang (fmyang@scu.edu.cn) and Mei Zheng (mzheng@pku.edu.cn)

Methodology

Sampling sites

The campaigns were performed simultaneously at PKU (116.32ºE, 39.99ºN) and PG (117.05ºE, 40.17ºN) from 11/01/2016 to 11/29/2016. A Description of the PKU site is available in the literature (Huang et al., 2006). Briefly, the site is located on the rooftop (15 m above the ground) on the PKU campus which is surrounded by residential and commercial blocks. Trace gases (Thermo Inc. series), meteorological parameters (Vaisala Inc.), and $PM_{2.5}$ (TEOM 1430) were recorded during the observation.

The PG site (117.053ºE, 40.173ºN) is 3 km from the PG center. The site is located in the northeast of the PKU site with a distance of 70 km. The PG site also acts as a host of the AIRLESS (Effects of AIR pollution on the cardiopulmonary disease in urban and peri-urban residents in Beijing) Project. The meteorological data is acquired from the local meteorological office. The PG village is surrounded by orchards and farmland with no main road nearby on a scale of 3 km. Coal and biomass are used for domestic heating and cooking in the nearby villages.

Instrumentation and data analysis

Two SPAMSs (Model 0515, Hexin Inc., Guangzhou, China) were deployed at both PKU and PG. A technical description of SPAMS is available in (Li et al., 2011). Briefly, a SPAMS has three functional parts: sampling, sizing, and mass spectrometry. In the sampling part, particles within a 0.1–2.0 μm size range pass efficiently through an aerodynamic lens. In the sizing unit, the aerodynamic diameter (D_{va}) is calculated using

the time-of-flight of particles. The particles are then decomposed and ionized into ions one-by-one using a 266 nm laser. A bipolar time-of-flight mass spectrometer measures the ions and generates the positive and negative mass spectra of each particle. The two instruments were maintained and calibrated following the standard procedures before sampling (Chen et al., 2017).

A neural network algorithm based on adaptive resonance theory (ART-2a) was used to resolve particle types from both datasets (Song et al., 1999). The parameters used were: a vigilance factor of 0.70, a learning rate of 0.05, and 20 iterations. This procedure generated 771 and 792 particle groups. Then, the groups were combined into particle types based on similar mass spectra, temporal trends, and size distributions (Dallosto and Harrison, 2006). During combining, relative areas of nitrate and sulfate were used to distinguish the stages of processing, assuming that more sulfate and nitrate can be measured if a particle is more processed during its lifetime. Thus, particles with relative peak areas of sulfate and nitrate larger than 0.1 were marked with nitrate (-Nit), sulfate (-Sul), respectively, or both. Finally, the strategy resulted in 20 and 19 particle types at PKU and PG respectively. Among them, 17 types appeared at both sites, and each type has identical mass spectra (R^2> 0.80) between each other.

Paritcle types overview

Table S1. Relative abundance of particle types in polluted and clear days at the PKU site

	E1	Clear1	E2	Clear2	E3	Clear2
BB_PKU	0.05	0.08	0.05	0.17	0.07	0.17
CA _PKU	0.00	0.00	0.01	0.00	0.00	0.00
EC-Nit_PKU	0.08	0.08	0.10	0.01	0.02	0.01
EC-Nit-Sul_PKU	0.12	0.09	0.13	0.05	0.08	0.05
EC-Sul_PKU	0.00	0.01	0.01	0.04	0.01	0.04
ECOC-Nit_PKU	0.03	0.04	0.03	0.01	0.02	0.01
ECOC-Nit-Sul_PKU	0.10	0.11	0.13	0.08	0.18	0.08
ECOC-Sul_PKU	0.06	0.14	0.13	0.28	0.18	0.28
Fe-rich_PKU	0.03	0.02	0.03	0.01	0.02	0.01
K-Amin-Nit_PKU	0.00	0.00	0.00	0.01	0.00	0.01
KAS_PKU	0.11	0.07	0.08	0.02	0.04	0.02
Ksec-Nit-Sul_PKU	0.22	0.20	0.12	0.12	0.12	0.12
Ksec-Sul_PKU	0.01	0.01	0.00	0.02	0.01	0.02
NaK_PKU	0.00	0.00	0.00	0.01	0.00	0.01
NaK-Nit_PKU	0.07	0.03	0.06	0.04	0.08	0.04
NaK-Nit-Sul_PKU	0.02	0.01	0.02	0.02	0.06	0.02
NaK-Sul_PKU	0.00	0.00	0.00	0.01	0.00	0.01
OC-Nit_PKU	0.01	0.01	0.01	0.01	0.01	0.01
OC-Nit-Sul_PKU	0.06	0.08	0.08	0.07	0.09	0.07
OC-Sul_PKU	0.01	0.01	0.01	0.02	0.01	0.02

Table S2. Relative abundance of particle types in polluted and clear days at the PG site

	E1	CLEAR1	E2	CLEAR2	E3	E4	CLEAR4
BB_PG	0.07	0.10	0.06	0.10	0.04	0.07	0.11
Ca-rich_PG	0.00	0.00	0.00	0.00	0.00	0.00	0.00
EC-Nit_PG	0.02	0.01	0.04	0.00	0.02	0.00	0.00
EC-Nit-Sul_PG	0.05	0.02	0.05	0.01	0.03	0.02	0.01
ECOC-Nit-Sul_PG	0.04	0.09	0.06	0.09	0.05	0.06	0.11
EC-Sul_PG	0.00	0.00	0.00	0.00	0.00	0.00	0.00
ECOC-Nit-Sul_PG	0.15	0.12	0.19	0.10	0.21	0.22	0.12
ECOC-Sul_PG	0.06	0.15	0.10	0.30	0.11	0.07	0.14
Fe-rich_PG	0.03	0.00	0.02	0.00	0.03	0.01	0.00
Ksec-Nit_PG	0.06	0.04	0.04	0.02	0.04	0.03	0.03
Ksec_Nit-Sul_PG	0.03	0.02	0.02	0.01	0.02	0.02	0.01
Ksec_PG	0.05	0.05	0.04	0.05	0.04	0.03	0.05
Ksec-Sul_PG	0.07	0.08	0.03	0.04	0.04	0.04	0.03
Nak-Nit_PG	0.02	0.01	0.01	0.00	0.01	0.03	0.01
Nak-Nit-Sul_PG	0.02	0.01	0.01	0.00	0.01	0.05	0.01
NaK_PG	0.02	0.03	0.02	0.02	0.01	0.02	0.03
NaK-Sul_PG	0.00	0.01	0.01	0.00	0.00	0.00	0.00
OC-Nit-Sul_PG	0.22	0.17	0.22	0.13	0.24	0.23	0.18
OC_PG	0.03	0.03	0.04	0.03	0.04	0.03	0.04
OC-Sul_PG	0.05	0.07	0.05	0.09	0.07	0.08	0.12

Table S3. Correlations of number fractions of particle types at PG.

	E1	CLEAR1	E2	CLEAR2	E3	E4	CLEAR4
E1	1.00						
CLEAR1	0.82	1.00					
E2	0.95	0.85	1.00				
CLEAR2	0.50	0.86	0.62	1.00			
E3	0.95	0.85	0.99	0.62	1.00		
E4	0.93	0.82	0.95	0.54	0.96	1.00	
CLEAR4	0.77	0.95	0.83	0.84	0.83	0.82	1.00

Mass Spectra

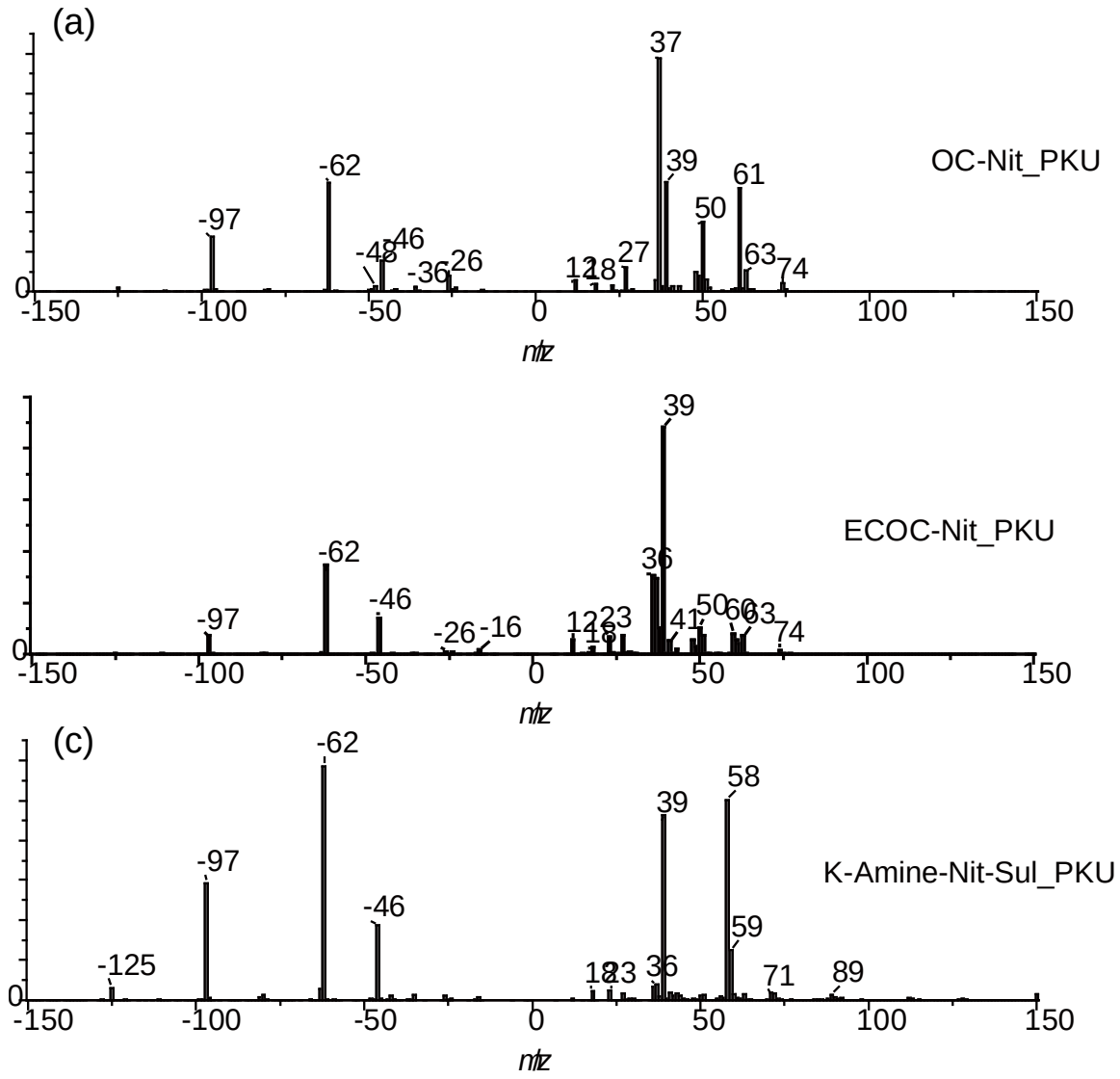

Figure S1. Unique Single particle mass spectra of particle types at PKU.

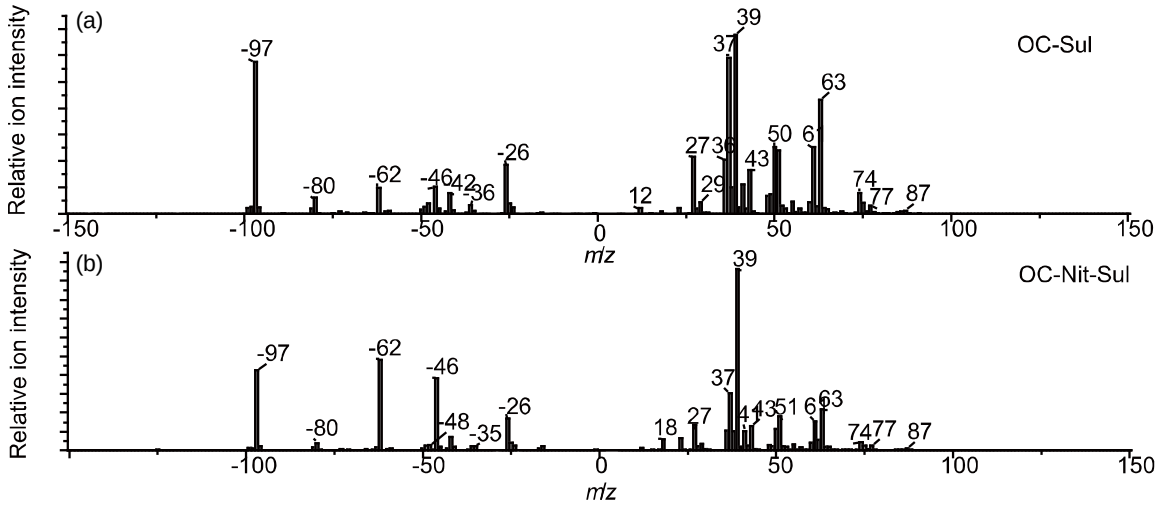

Figure S2. Single particle mass spectra of OC-related particle types at both PKU and PG.

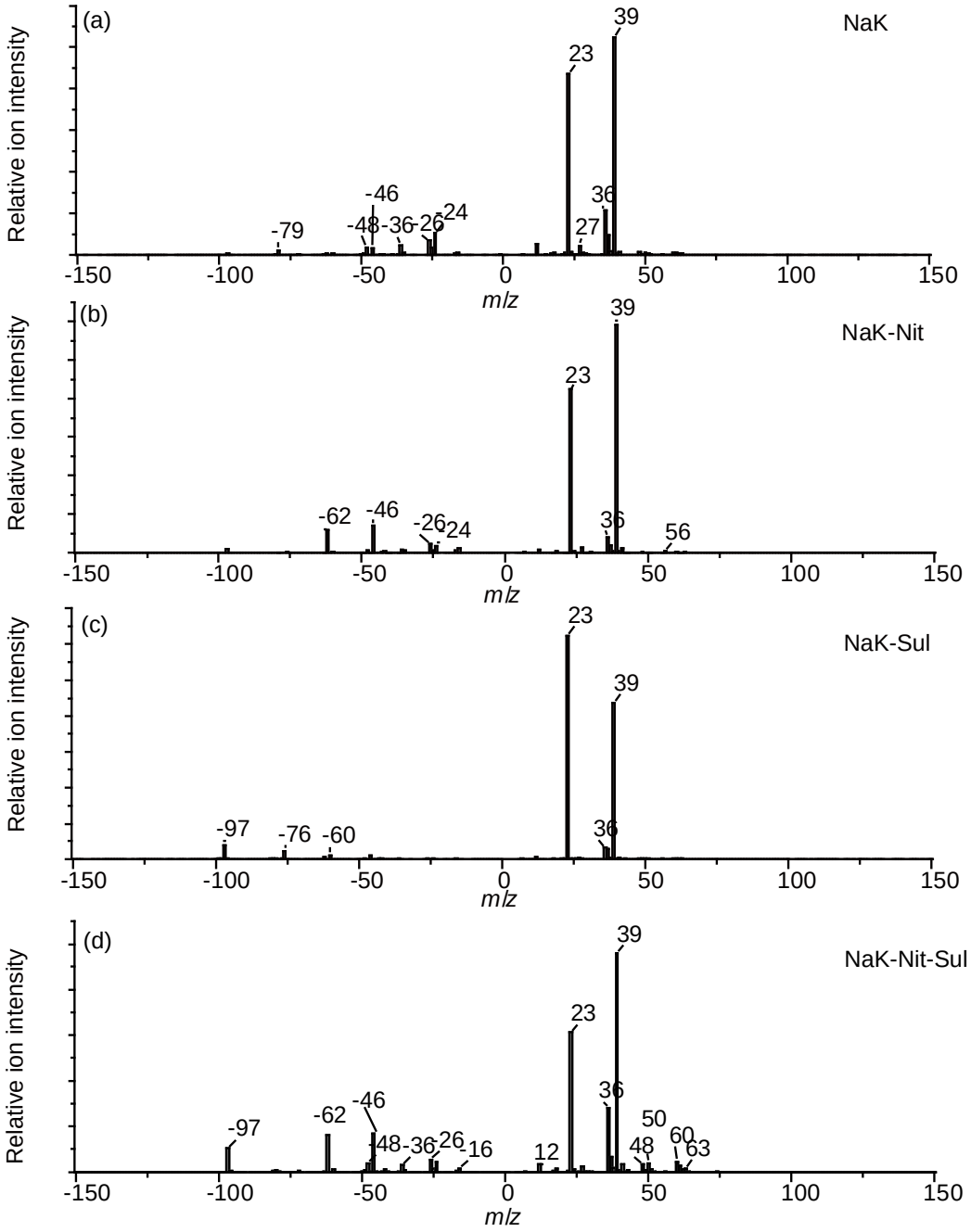

Figure S3. Single particle mass spectra of NaK-related particle types at both PKU and PG.

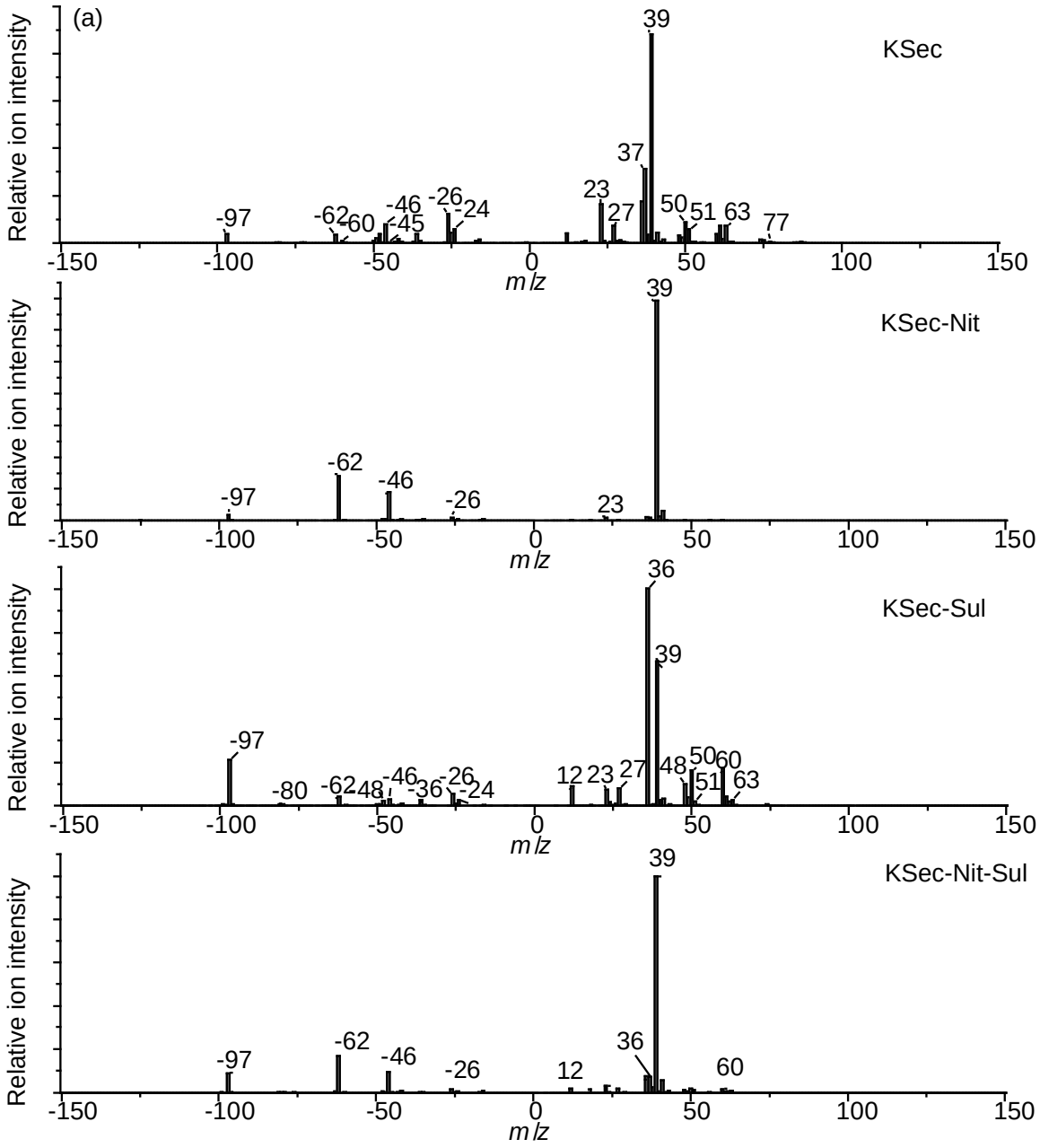

Figure S4. Single particle mass spectra of KSecondary-related particle types at both PKU and PG.

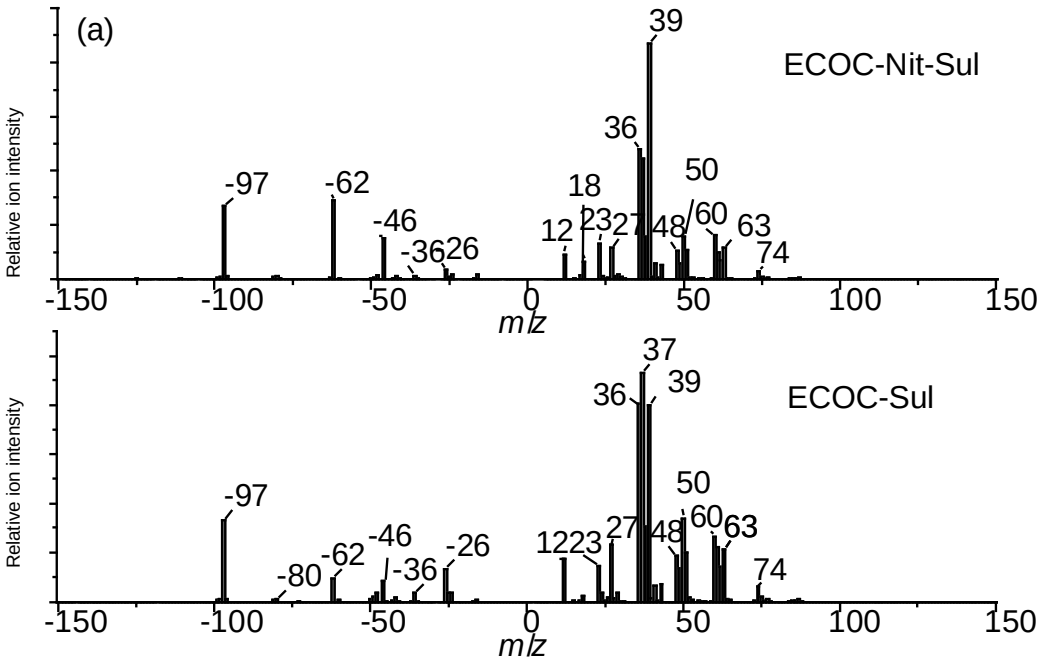

Figure S5. Single particle mass spectra of ECOC-related particle types at both PKU and PG.

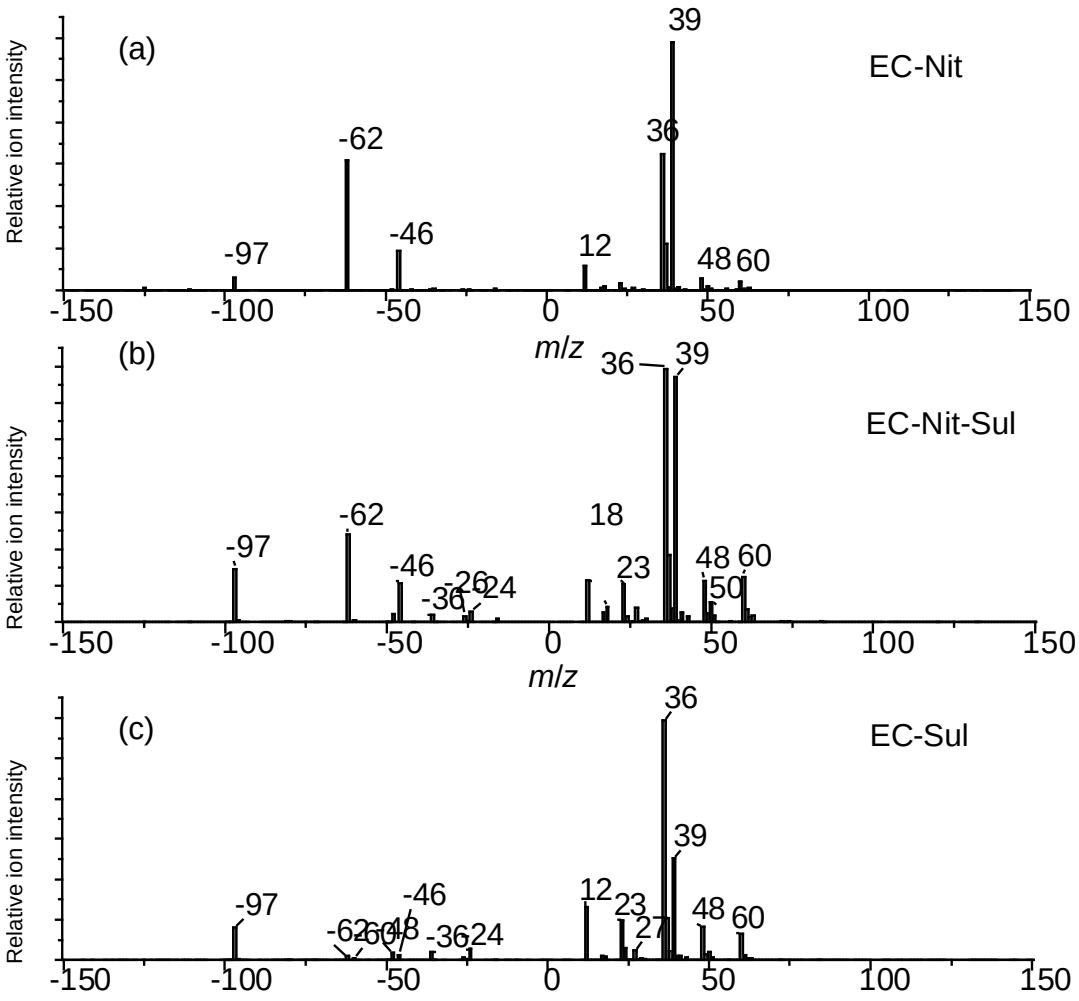

Figure S6. Single particle mass spectra of EC-related particle types at both PKU and PG.

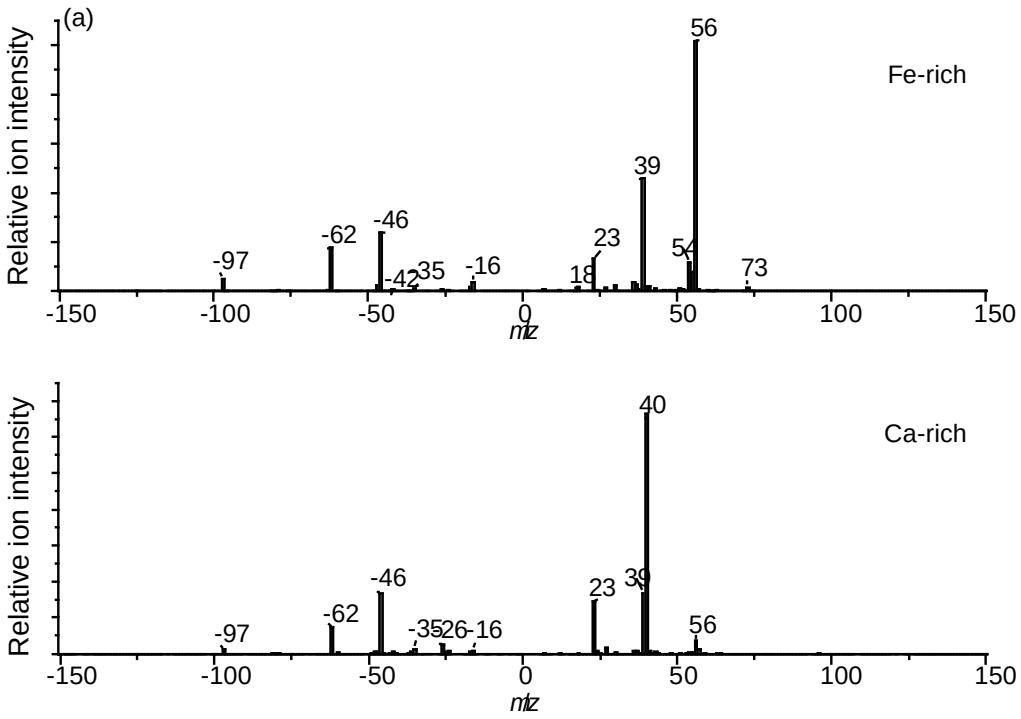

Figure S7. Single particle mass spectra of metal-related particle types at both PKU and PG.

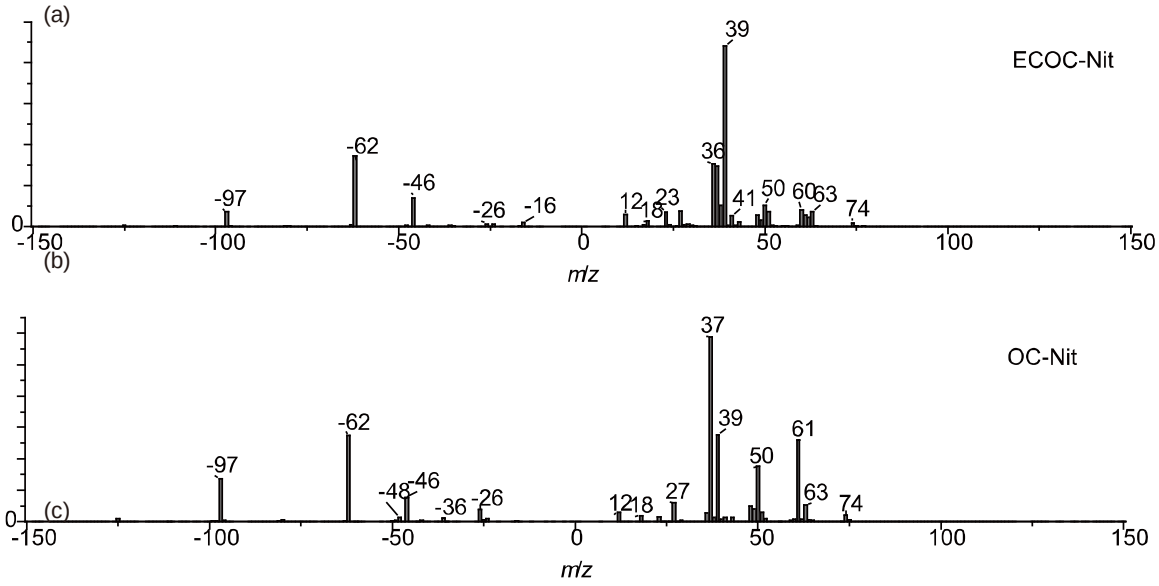

Figure S8. Single particle mass spectra of Nitrate-rich particle types at PKU.

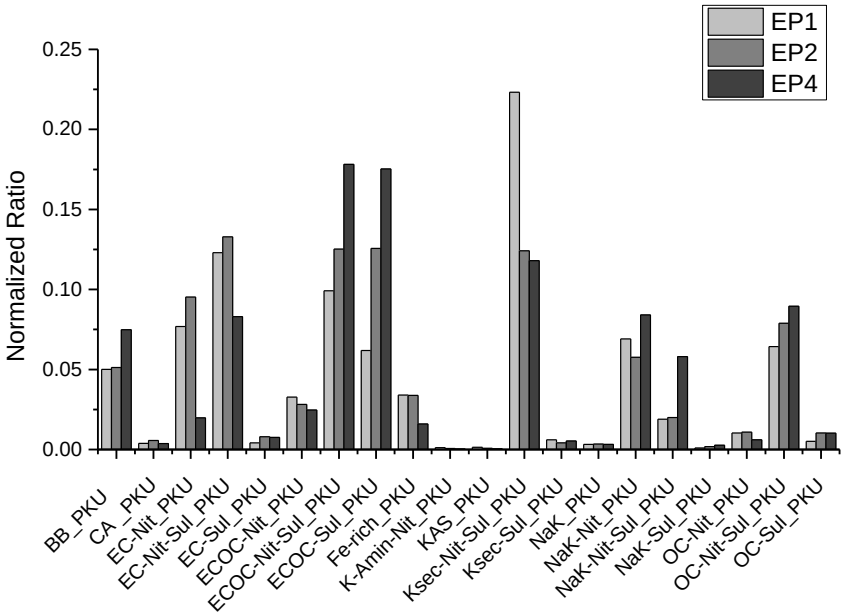

Figure S9. Normalized ratios of particle types at PKU during three pollution events.

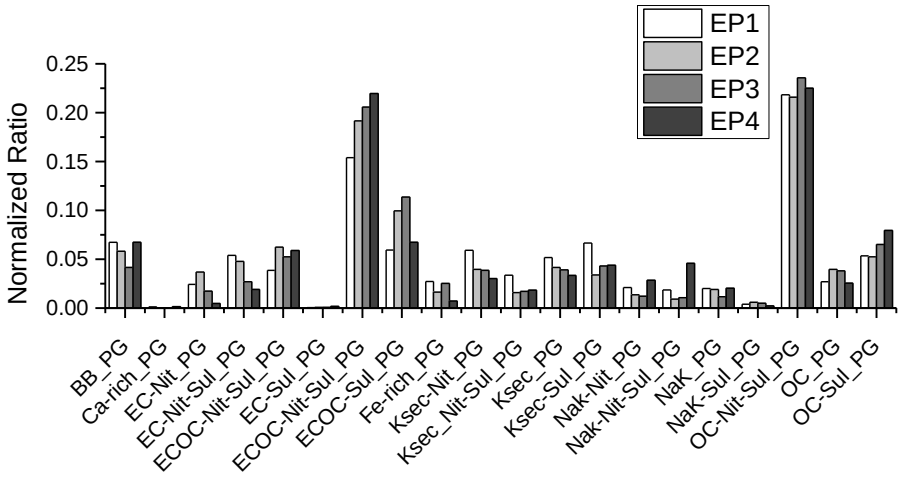

Figure S10. Normalized ratios of particle types at PG during four pollution events.

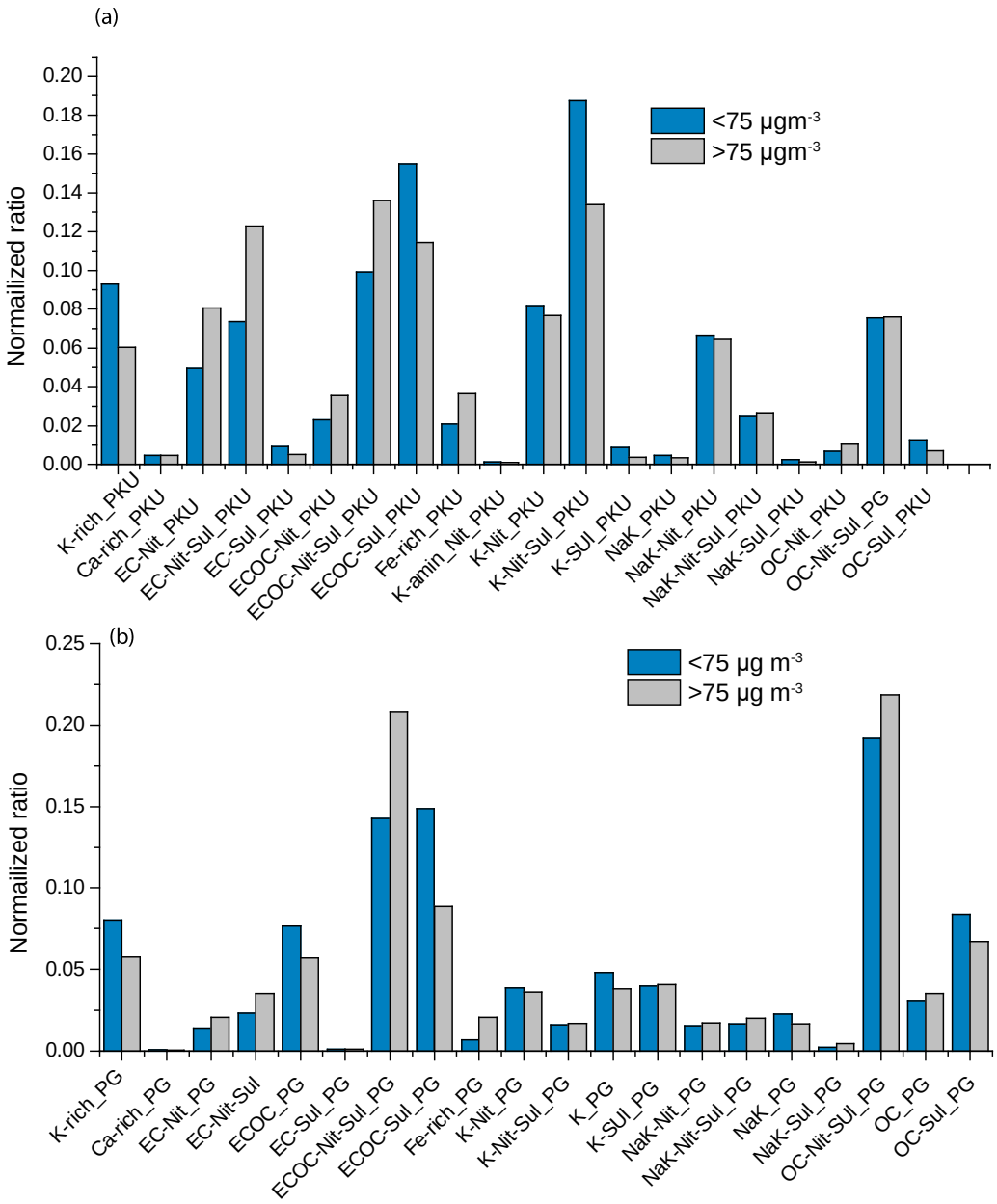

Figure S11. The relative abundance of normalized number ration of particle types in the pollution events and adjacent clear days.

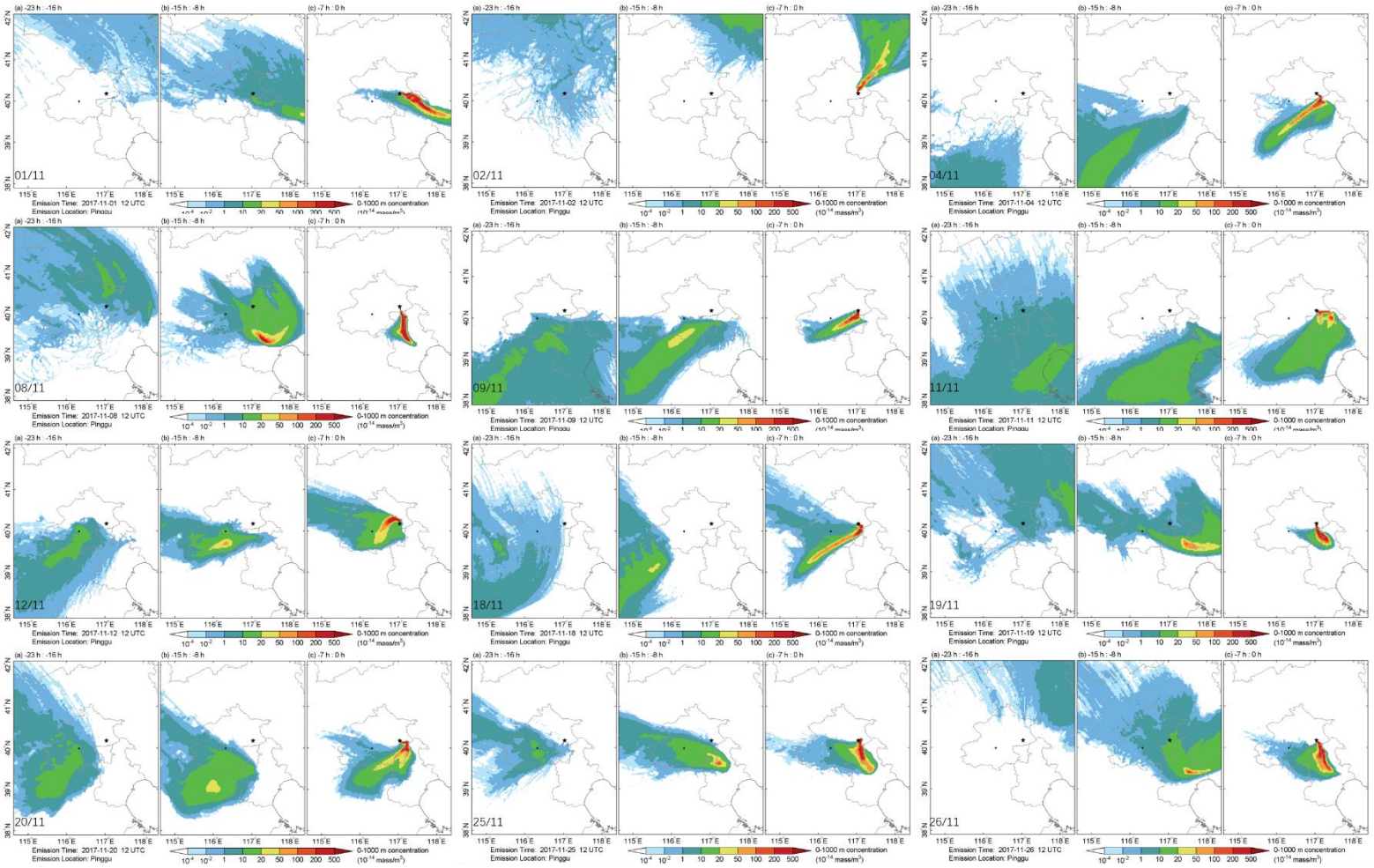

Figure S11. Air mass dispersed from PG (star, on the right) to PKU (dot, on the left) during the observation period.

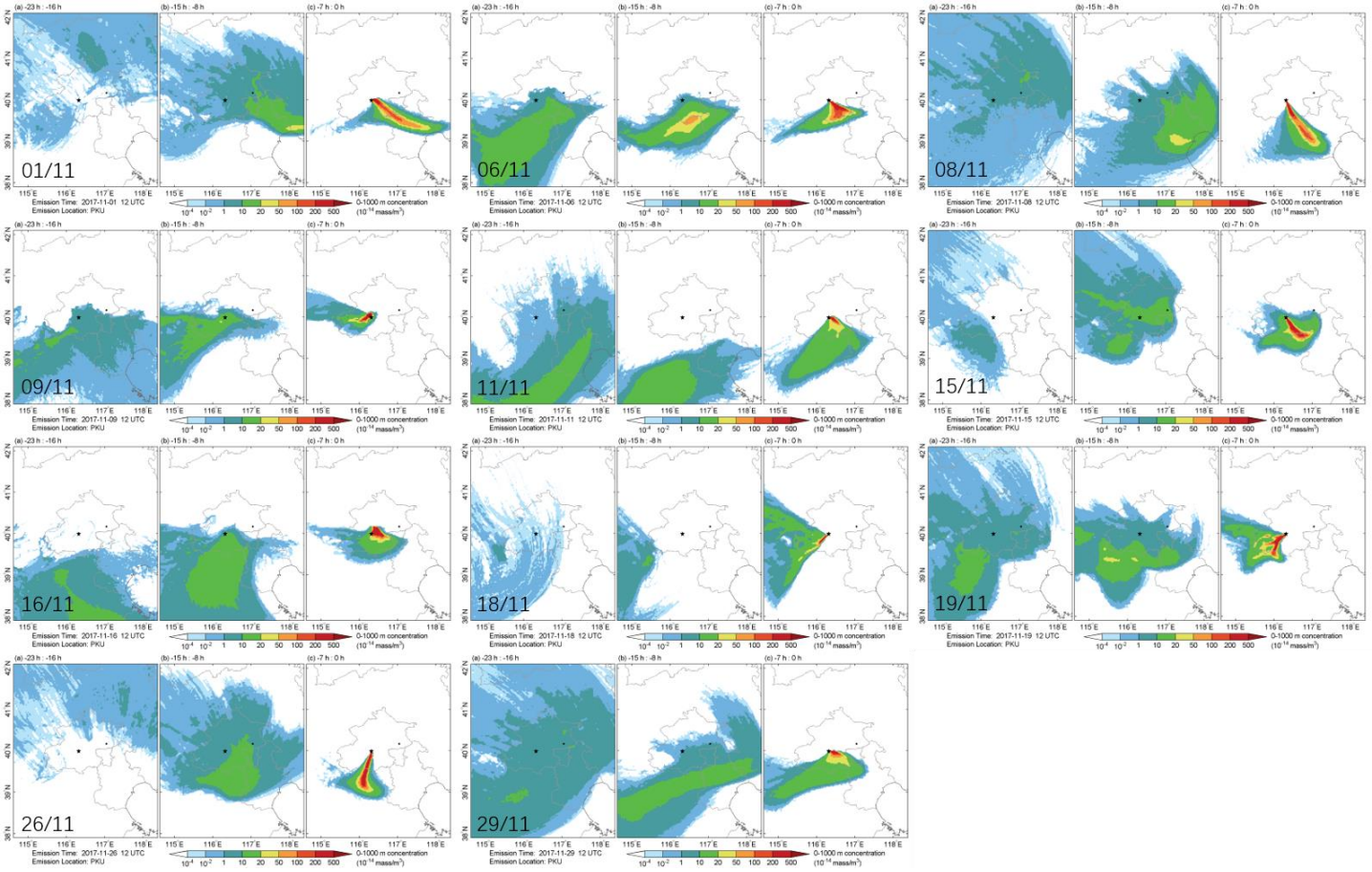

Figure S12. Air mass dispersed from PKU (star, on the left) to PG (dot, on the right) during the observation period.